Korean J. Chem. Eng., **26**(4), 1098-1105 (2009)
DOI: 10.1007/s11814-009-0183-x

Monte Carlo simulation on the adsorption properties of carbon tetrachloride, neopentane, and cyclohexane in MCM-41

Sung Doo Moon*,† and Dae Woong Choi**

*Department of Chemistry, Pukyong University, Busan 608-737, Korea
**Department of Chemical Engineering, Dongeui University, Busan 614-010, Korea
(*Received 5 August 2008 • accepted 29 December 2008*)

Abstract−The adsorption properties of carbon tetrachloride, neopentane, and cyclohexane in MCM-41 with heterogeneous and cylindrical pores have been studied by using grand canonical ensemble Monte Carlo simulation. The adsorption isotherm, average potential of adsorbate, isosteric heat of adsorption, and number density of molecules in MCM-41 were calculated. The simulated isotherms were compared with experimental ones. Also, different adsorption behaviors in MCM-41 with pore diameter of 2.2 and 3.2 nm were discussed. The capillary-condensation pressure increased for a given adsorbate with an increase in pore diameter. The average densities of carbon tetrachloride, neopentane, and cyclohexane in the two different pores above the capillary-condensation pressure were smaller than the corresponding liquid densities by about 12%. The adsorbate molecules did not form the multilayer in pore below the capillary-condensation pressure. The number of adsorption layers of molecules was constant in a given pore for the three adsorbates above the capillary-condensation pressure. Carbon tetrachloride molecules in pore were also ordered along the pore axis.

Key words: Adsorption, MCM-41, Monte Carlo, Carbon Tetrachloride, Neopentane, Cyclohexane

INTRODUCTION

MCM-41, one member of the M41S family, possesses highly regular arrays of uniform-sized channel whose diameters are in the range of 1.5-10 nm, depending on the templates used, the addition of auxiliary organic compounds, and the reaction parameters [1]. MCM-41 is one of the most widely studied among the numerous mesoporous materials because of its structural simplicity and ease of preparation with negligible pore-networking and pore blocking effects [2]. Hence, adsorption properties of molecules in MCM-41 have been extensively investigated.

Simulation-based techniques, which can be used to predict the behavior of molecules at conditions for which experimental data are difficult or impossible to obtain, provides significantly more reliable results than is possible with approximate theoretical methods [3]. Monte Carlo (MC) techniques have been developed to sample the configurations. Especially the configurational bias Monte Carlo (CBMC) technique accelerates the equilibration of a dense system, in which insertion attempts are biased toward favorable regions [4]. This technique has shown to improve in the efficiency of simulations compared to normal MC simulations.

Grand canonical ensemble Monte Carlo (GCMC) simulation, in which the chemical potential, temperature, and volume of system are fixed, has been used to investigate adsorption of molecules in porous materials such as zeolite and carbon nanotube [5,6]. The GCMC simulations for nitrogen, hexane, 2-methyl pentane, cyclohexane in hexagonal nanopores of MCM-41 have been performed [7,8]. The GCMC simulations for argon, krypton, nitrogen, carbon dioxide, methane, ethane, carbon tetrachloride in cylindrical nanopores of MCM-41 have been reported [9-15]. Also, the adsorption of carbon dioxide in slit-like silica nanopore using GCMC simulation was reported [16]. On the other hand, the effect of surface roughness on the adsorption properties has been studied by MC simulation. Coasne and Pellenq reported that the adsorption amounts of argon in a rough pore were larger than those in a smooth pore [17]. They showed that the difference between the two adsorption amounts was constant at all pressures and was due to adsorption of argon at very low pressure in the infractions of the rough surface which acted as a microporous texture. Coasne et al. reported that surface disorder induced a decrease in the capillary-condensation pressure [18].

The MC simulations on the adsorption properties in MCM-41 have been mainly studied for small molecules or simply modeled molecules. The aim of this study is to calculate the adsorption isotherm, adsorption potential, isosteric heat, and distributions of number densities for carbon tetrachloride, neopentane, and cyclohexane by GCMC simulation in which the molecule is modeled explicitly. In the following section the details of the MCM-41 model, the molecular model, and the simulation method are described. Thereafter, the simulation results are presented, compared with the experimental values, and discussed.

MODELS

We modeled the structure of MCM-41 with heterogeneous and cylindrical pore using a technique similar to that in the cited literature [12]. First, oxygen and silicon atoms in 2 : 1 stoichiometry were placed in a rectangular box of $5.6\times5.6\times1.6\ nm^3$ such a way that the skeletal density was $2.2\ g/cm^3$, which corresponds to the density of amorphous silica. Then, the atoms were randomly mixed with the following restrictions. (1) The distance between oxygen and silicon atoms cannot be less than the bond distance of oxygen and silicon

†To whom correspondence should be addressed.
E-mail: sdmoon@pknu.ac.kr

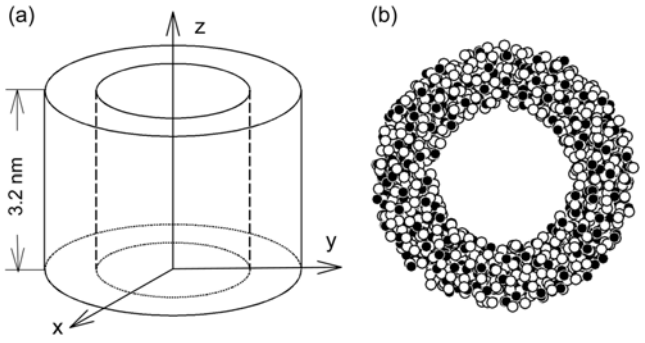

Fig. 1. (a) The geometry of the simulation box of MCM-41 model. The z axis is taken along the pore axis. (b) Top view of the pore of MCM-41 model. Closed and open circles denote silicon and oxygen atoms, respectively.

Table 1. Potential parameter for carbon tetrachloride, neopentane, cyclohexane, and MCM-41

Site	σ(nm)	ε/k(K)	q(e)
C (carbon tetrachloride[a])	0.3774	27.4	−0.696
Cl (carbon tetrachloride[a])	0.3467	131.7	0.174
CH_3 (neopentane[b])	0.396	73	0
C (neopentane[b])	0.380	52.9	0
CH_2 (cyclohexane[c])	0.39	70	0
O (MCM-41)	0.2708[d]	101.6[d]	−0.18[d]
Si (MCM-41)	0	0	0.36[d]

[a]Rey et al. [21]
[b]de Pablo et al. [20]
[c]Gupta et al. [22]
[d]Koh et al. [10]

atoms (0.163 nm) [19]. (2) The distance between two silicon atoms cannot be less than that in Si-O-Si structure (0.31 nm) [19]. (3) The distance between two oxygen atoms cannot be less than that in O-Si-O structure (0.266 nm) [19]. Then we carved out the rectangular box in order to obtain a cylindrical structure with pore diameter of 3.2 nm, pore length of 1.6 nm, and wall thickness of 0.95 nm. This wall thickness corresponds to the average value for siliceous MCM-41 [1]. When the ratio of the number of silicon atoms to that of oxygen atoms in the cylindrical structure was not 1 : 2 and the density of the structure was not 2.2 g/cm^3, we again carved out another place of the rectangular box until a cylindrical structure with the conditions mentioned above was obtained. Finally, we connected two of the cylindrical structures lengthwise in order to make simulation box with pore length of 3.2 nm. The simulation box consisted of 2,622 atoms of oxygen and silicon. On the other hand, by similar method, we made the other simulation box with pore length of 3.2 nm, pore diameter of 2.2 nm, and wall thickness of 0.95 nm, which consisted of 1,988 atoms of oxygen and silicon. Fig. 1 shows the geometry of the simulation box and top view of the pore of MCM-41 model.

The nonbonded interaction between two sites were calculated by Coulombic and Lennard-Jones (LJ) potential:

$$u_{ab}=\frac{q_a q_b}{r_{ab}}+4\varepsilon_{ab}\left[\left(\frac{\sigma_{ab}}{r_{ab}}\right)^{12}-\left(\frac{\sigma_{ab}}{r_{ab}}\right)^{6}\right] \quad (1)$$

where r_{ab} is the distance between *a* site and *b* site and q_a is a partial charge located at *a* site. ε_{ab} and σ_{ab} were obtained with the standard Lorentz-Berthelot combining rules given by

$$\sigma_{ab}=0.5(\sigma_a+\sigma_b) \text{ and } \varepsilon_{ab}=\sqrt{\varepsilon_a \varepsilon_b} \quad (2)$$

CH_3 and CH_2 groups in adsorbate molecule were considered as single interaction pseudo-atoms located at the center of carbon atoms. Bond lengths and bond angles were fixed in simulation. The nonbonded interaction in the same molecule was not considered. The geometries of the adsorbate molecules were adopted as follows: r(CH_3-C)= 0.153 nm and ∠CCC=109.47° for neopentane [20], r(C-Cl)=0.1766 nm and ∠ClCCl=109.47° for carbon tetrachloride [21], r(CH_2-CH_2) =0.154 nm and ∠CCC=109.47° for cyclohexane [22]. Cyclohexane molecule was assumed to be only chair conformation. The LJ parameter and the potential charge of site are summarized in Table 1. The positions of silicon and oxygen atoms of MCM-41 model were fixed throughout the simulation because MCM-41 structure is thermally stable except for high temperature. The contribution of silicon to the LJ potential was not considered because the polarizability of silicon atom is very small and correspondingly its dispersion interaction is negligible.

In general, a pair potential with a spherical cutoff is used to reduce the computing time in simulations. In this case, it becomes necessary to correct the results of simulations to compensate for the missing long-range part of the potential. To calculate the potential between a site of adsorbate molecules and MCM-41 including the long-range contribution, ϕ_{sm}, we used a large structure of MCM-41 whose pore length was 8.0 nm. This structure of MCM-41 was electrically neutral, and the simulation box was placed at the center of the structure. ϕ_{sm} was calculated by a full image convention. This implies that ϕ_{sm} is the potential between a site of adsorbate molecules and all the atoms in the MCM-41 structure. To verify that the structure was large enough, we compared the potentials and adsorption amounts of carbon tetrachloride in the MCM-41 structure with those calculated in a larger MCM-41 structure with pore length of 11.2 nm at 298 K. The potentials between carbon tetrachloride and the MCM-41 structure with pore length of 11.2 nm and pore diameter of 2.2 nm were −23.7, −24.5, −24.5, and −24.4 kJ/mol at 2.0, 3.0, 9.8, and 12 kPa, respectively. Those with pore length of 8.0 nm and pore diameter of 2.2 nm were −24.6, −24.8, −25.0, and −24.4 kJ/mol at 2.0, 3.0, 9.8, and 12 kPa, respectively. The simulated adsorption amounts of carbon tetrachloride for the two structures were the same at constant pressure. As a result, there was almost no effect of the size of MCM-41 structure on the adsorption properties.

To reduce the calculation time of ϕ_{sm} the following simplification was introduced. After the simulation box was divided into a large number of cells, ϕ_{sm} was calculated at the center of each divided cell and stored. ϕ_{sm} of a site of molecules placed in a certain divided cell was assumed to be that one calculated at the center of the divided cell. Volume of the divided cell was 8×10^{-6} nm^3. To check if this volume was small enough or not, the method was applied to the calculation of the thermodynamic properties of carbon tetrachloride, and the results were compared with those obtained for smaller volume of the cell (4.5×10^{-6} nm^3). Practically identical results were obtained. For the LJ part of the potential of adsorbate/adsorbate,

the spherical cutoff was 1.5 nm, and the potential arising from truncation was not corrected. We did not apply the spherical cutoff and its correction to the calculation of the Coulombic potential of adsorbate/adsorbate. Instead all the sites of molecules in simulation box were considered in calculation of the Coulombic potential of adsorbate/adsorbate in order to avoid the incorrectness of calculation causing from the electrical unneutrality in space within cutoff distance.

SIMULATION METHOD

Five types of trial moves in this study were as follows: (a) molecule translation, (b) molecule rotation, (c) inserting molecule, (d) removing molecule, and (e) regrowing molecule. Move (e) was employed because it is difficult to successfully move large molecules in normal MC simulations.

In move (b), a molecule was selected at random and was rotated. The center of the rotation was at the center of a molecule, and the molecule was randomly rotated [23] about an axis parallel to a randomly chosen coordinate axis shown in Fig. 1. In move (a) and (b), the trial moves were accepted with probability given by

$$P_{acc}=\min[1, \exp(-\beta\Delta u)] \tag{3}$$

where Δu is the energy change for the trial move, and β is 1/kT. Here k is Boltzmann constant and T is temperature. Move (c), (d), (e) were performed by using the methods given in the cited literature [4,23-25]. In move (c), a molecule was inserted by the following three steps. (1) At the first step (i=1), a random position of the first site was generated and the energy of this site, u_1, was calculated. (2) At the second step (i=2), m locations for the second site were randomly generated on the surface of a sphere. The radius of this sphere was the bond length between the first and the second sites, and the center of the sphere was located at the first site. One of these positions was selected with probability,

$$p_i(b_j)=\frac{\exp[-\beta u_i(b_j)]}{w_i^{(n)}} \tag{4}$$

$$w_i^{(n)}=\sum_{j=1}^{m}\exp[-\beta u_i(b_j)] \tag{5}$$

where m is the total number of trials, the u_i is the energy due to inserting the second site in position b_j. (3) At the final step (i=3), the remaining sites were rotated around the axis formed by the first and the second sites. m rotations were generated after which the rotations of the remaining sites were selected with the probability given by Eq. (4). The move (c) was accepted with probability [26],

$$P_{acc}=\min\left(1, \frac{f\beta V}{(N+1)}W^{(n)}\right) \tag{6}$$

$$W^{(n)}=\exp(-\beta u_1)\prod_{i=2}^{3}\frac{w_i^{(n)}}{m} \tag{7}$$

where N is the number of molecules in the simulation box, V is the volume of the simulation box, $W^{(n)}$ is the new Rosenbluth factor. The fugacity of the vapor phase, f, was calculated by ln(f/P)=BP/RT, where P is pressure and R is gas constant. The virial coefficient, B, was estimated from the cited literature [27]. The move (d) was performed by a method similar to move (c). A randomly selected molecule was removed by using the following three steps. (1) The energy of the first site of the selected molecule, $u_1^{(o)}$, was calculated. (2) m−1 locations for the second site were randomly generated as in the second step of move (c). $w_i^{(o)}$ was calculated by

$$w_i^{(o)}=\exp(-\beta u_i^{(o)})+\sum_{j=2}^{m}\exp[-\beta u_i(b_j)] \tag{8}$$

where $u_i^{(o)}$ is the energy of the second site of the selected molecule. (3) As in move (c), the remaining sites were rotated around the axis formed by the first and the second sites of the selected molecule. m−1 rotations were generated, and $w_i^{(o)}$ was calculated by Eq. (8). The move (d) was accepted with probability [26],

$$P_{acc}=\min\left(1, \frac{N}{f\beta V}\frac{1}{W^{(o)}}\right) \tag{9}$$

$$W^{(o)}=\exp(-\beta u_1^{(o)})\prod_{i=2}^{3}\frac{w_i^{(o)}}{m} \tag{10}$$

$W^{(o)}$ is the old Rosenbluth factor. In move (e), a randomly selected molecule was cut at a randomly selected site, at which regrowing began. The regrowth was accepted with probability given by Eq. (11).

$$P_{acc}=\min(1, W^{(n)}/W^{(o)}) \tag{11}$$

The calculations of $W^{(n)}$ and $W^{(o)}$ in move (e) were similar to those in Eqs. (7) and (10), respectively, where i is determined by the regrowing site. For instance, if all the sites of a molecule were regrown, the values of $W^{(n)}$ and $W^{(o)}$ in Eq. (11) would be equal to those in Eqs. (7) and (10), respectively. In this study, the u included only the nonbonded interaction potential calculated by Eq. (1) because the bond lengths and bond angles were fixed. m was set to 10 in moves (c), (d), and (e).

Periodic boundary condition was used only along the pore axis in simulation, and simulations were performed in MC cycles. In each MC cycle, first, trial moves equal to 30 times the number of molecules in simulation box occurred with the following probabilities: 30%, 30%, and 40% for move (a), (b), and (e), respectively; then either a move (c) or a move (d) was attempted. For moves (a) and (b), the maximum move was adjusted to give an average acceptance ratio of 40% every 100 MC cycles. 1×10^3–1.8×10^4 MC cycles were discarded before 4×10^3 MC cycles for equilibrium were performed. The thermodynamic properties of the system were calculated by accumulating the computed properties every MC cycle and by averaging them. The initial configurations below the capillary-condensation pressure were obtained by NVT simulation, which consisted of moves (a), (b), and (e). In the NVT simulation the number of molecules was 10 and 20 in the simulation box of MCM-41 with pore diameter of 2.2 and 3.2 nm, respectively. For the system above the capillary-condensation pressure, the last configuration of each run was used as the initial configuration of the next run to equilibrate fast.

RESULTS AND DISCUSSION

Fig. 2 shows the ratio of the number of silicon atoms to that of oxygen atoms as a function of distance from the pore axis of MCM-41 with pore diameter of 2.2 and 3.2 nm, indicating that the pore wall of the model is almost amorphous.

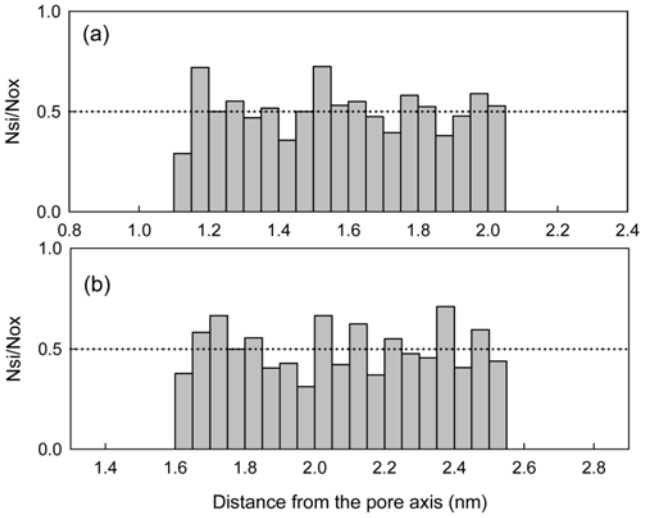

Fig. 2. The ratio of the number of silicon atoms to that of oxygen atoms, Nsi/Nox, as a function of distance from the pore axis of MCM-41 with pore diameter of (a) 2.2 and (b) 3.2 nm.

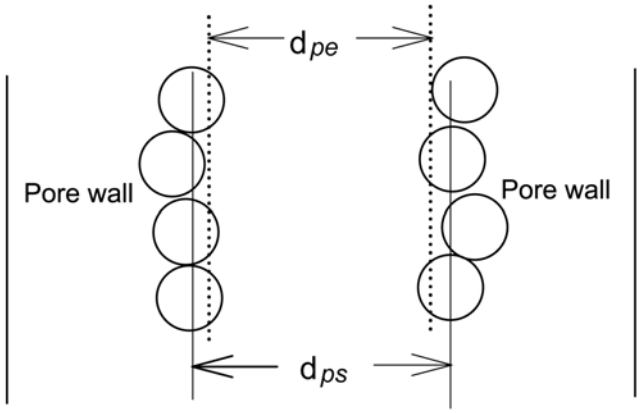

Fig. 4. Schematic of lateral view of the cylindrical pore. d_{ps} is pore diameter in simulation. The pore diameter measured in experiment, d_{pe}, is less than d_{ps} by a half of σ of oxygen atom. Open circle denotes oxygen atom on surface of wall.

Fig. 3 shows the experimental and simulated adsorption isotherms of carbon tetrachloride at 298 K, neopentane at 273 K, and cyclohexane at 298 K in MCM-41 with pore diameter of 3.2 and 2.2 nm. Here P_{sat} denotes the saturated vapor pressure. Only the simulated isotherm is plotted in Fig. 3(c) because we were not able to find the experimental isotherm of cyclohexane with which to compare directly the simulated one. The experimental adsorption amounts of carbon tetrachloride and neopentane were estimated from the cited literature [28,29]. The pore diameter in the experiment does not correspond to that in simulation. The reason is that the adsorbate molecules cannot get access to the pore wall due to the volume of the oxygen atom on the surface of pore. Therefore, we assumed that the pore diameter in the experiment was less than that in simulation by a half of σ of oxygen atom as shown in Fig. 4.

To compare the experimental adsorption amounts with the simulation results, the porosity was taken as a conversion factor. As the pore wall thickness of MCM-41 is in the range of 0.8-1.1 nm [1], the pore wall thickness of the MCM-41 model was not used for conversion [11]. In this study, we plotted the porosity measured by N_2 BET experiment as a function of the pore diameter measured by N_2 BET experiment, and estimated the porosity corresponding to the pore diameter of the MCM-41 model from the slope of line in this plot. We used the experimental data given by Hakuman and Naono [28] to obtain the porosity of the MCM-41 model for the adsorption of carbon tetrachloride, and by Carrott et al. [29] to obtain that for the adsorptions of neopentane and cyclohexane.

Fig. 3 shows that the capillary-condensation pressure increases for a given adsorbate with an increase in pore diameter. The simulated isotherm of neopentane above the capillary-condensation pressure agrees with the experimental one. However, the simulated adsorption amounts of carbon tetrachloride above the capillary-condensation pressure in MCM-41 with pore diameter of 2.2 and 3.2 nm are less than the experimental ones by 5% and 16%, respectively. Fig. 3(b) shows that the capillary-condensation pressure in simulation differs from that in experiment, and that the difference in the adsorption amounts between simulation and experiment is large at low P/P_{sat}. The discrepancies result from several factors. The main reason may be that the heterogeneity of the adsorbent is

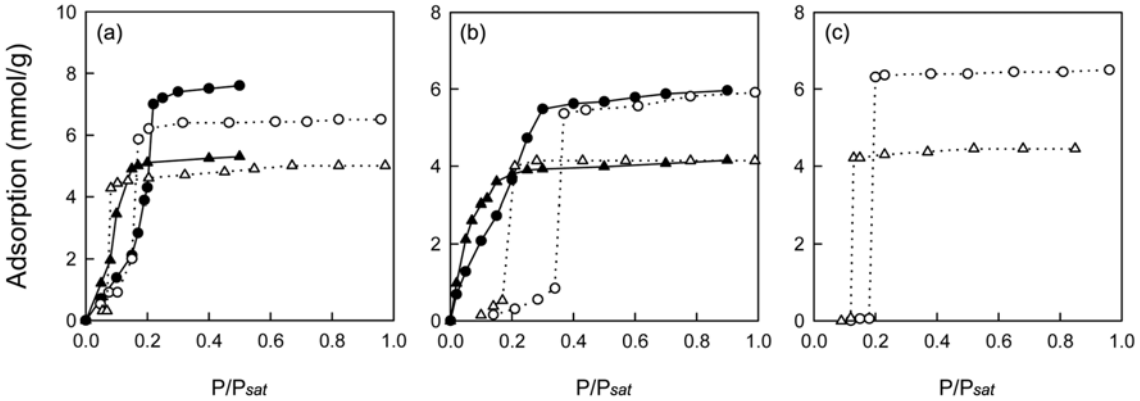

Fig. 3. The experimental (closed points) and simulated (open points) adsorption isotherms in MCM-41 with pore diameter of 3.2 (circle points) and 2.2 nm (triangle points): (a) carbon tetrachloride at 298 K, (b) neopentane at 273 K, and (c) cyclohexane at 298 K. Solid and dot lines are guides for the eye.

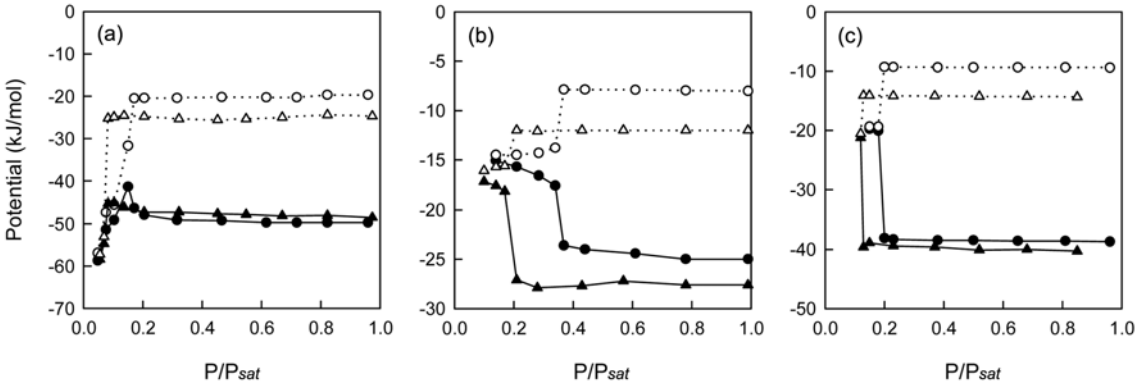

Fig. 5. The total potential (closed points) and the potential of adsorbate/adsorbent (open points) in MCM-41 with pore diameter of 2.2 (triangle points) and 3.2 nm (circle points): (a) carbon tetrachloride at 298 K, (b) neopentane at 273 K, and (c) cyclohexane at 298 K. Solid and dot lines are guides for the eye.

not considered enough. For instance, Fox and Bates reported that the discrepancies were attributed to omitting the micropore on the pore wall of MCM-41 model [8]. He and Seaton showed that the simulated adsorption isotherms of ethane, carbon dioxide, and their mixture in MCM-41 with amorphous structure were in agreement with the experimental ones better than those in MCM-41 with homogeneous structure or crystalline quartz structure [12]. Muller et al. reported that the adsorption behavior of water in activated carbon pore was strongly dependent on the density of the activated site on the pore [30]. According to their study, the simulated adsorption amounts of water were almost negligible below the capillary-condensation pressure, and the capillary-condensation pressure increased with a decrease in the site density. These adsorption behaviors are very similar to those in Fig. 3(b), suggesting that the adsorptive sites interacting with neopentane in our model of MCM-41 are less than those in the real structure. The MCM-41 model with a heterogeneous surface on which there are a variety of sites, from highly attractive to standard silica-type sites, is needed to accurately predict the adsorption amounts, especially at low pressure [9]. Additionally, it may be necessary to consider the surface silanol, distribution of pore size, and variation of pore wall thickness.

Fig. 5 shows the total potential and the potential of adsorbate/adsorbent in MCM-41 with pore diameter of 2.2 and 3.2 nm. The potential of adsorbate/adsorbate corresponds to the difference between the total potential and the potential of adsorbate/adsorbent. Fig. 5 shows that the potential of adsorbate/adsorbent is almost the same as the total potential at very low P/P_{sat}, indicating that the molecules are adsorbed in the region close to the pore wall at very low P/P_{sat}. Also the figure shows that the interaction between the adsorbate and the adsorbent with narrow pore is stronger than that with large pore. Below the capillary-condensation pressure, the potential of adsorbate/adsorbent increases with the adsorption amount increase. This is because molecules to be adsorbed at high P/P_{sat} are located farther from the wall than those at low P/P_{sat}. The total potential of carbon tetrachloride initially increases with increasing of P/P_{sat} until it reaches the peak of potential, and then decreases very slowly. There are no peaks of potential for neopentane and cyclohexane. The peak of the total potential of carbon tetrachloride appears because the potential of carbon tetrachloride/adsorbent increases steeply at very low P/P_{sat} while the potential between carbon tetrachloride molecules decreases.

We calculated the isosteric heat in pore, q_{st}, at high P/P_{sat} using Eq. (12) [22]:

$$q_{st} = RT - \langle U \rangle - \langle N \rangle \left(\frac{\partial \langle U \rangle}{\partial \langle N \rangle} \right)_{T,V} \tag{12}$$

where U is the potential of adsorbate. The q_{st} for pore diameter of 3.2 nm was 52.2, 27.3, and 41.1 kJ/mol for carbon tetrachloride at $P/P_{sat}>0.82$, neopentane at $P/P_{sat}>0.78$, and cyclohexane at $P/P_{sat}>0.81$, respectively. The q_{st} for pore diameter of 2.2 nm was 50.7, 30, and 42.7 kJ/mol for carbon tetrachloride at $P/P_{sat}>0.82$, neo-

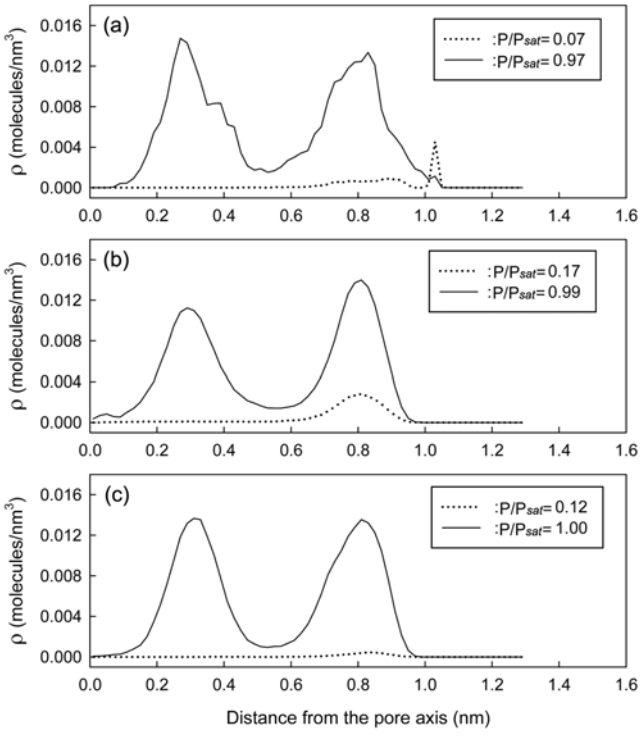

Fig. 6. Number density of molecules, ρ, in MCM-41 with pore diameter of 2.2 nm as a function of distance from the pore axis: (a) carbon tetrachloride at 298 K, (b) neopentane at 273 K, and (c) cyclohexane at 298 K.

pentane at $P/P_{sat}>0.78$, and cyclohexane at $P/P_{sat}>0.7$, respectively. On the other hand, the heats of condensation in bulk of carbon tetrachloride, neopentane, and cyclohexane are 32.43, 22.74, and 33.01 kJ/mol, respectively [31]. The average densities of carbon tetrachloride, neopentane, and cyclohexane in the two different pores above the capillary-condensation pressure were 1.35, 0.55, and 0.69 g/cm^3, respectively. These values are smaller than the corresponding liquid densities by about 12%, which suggests that the interaction between molecules in bulk is stronger than that in pore. However, the q_{st} is higher than the heat of condensation in bulk. This is due to the fact that the interaction between adsorbate and adsolvent contributes greatly to the q_{st}. The difference between the q_{st} and the heat of condensation in bulk of carbon tetrachloride is larger than that of neopentane or cyclohexane, indicating that carbon tetrachloride interacts most strongly with MCM-41 among the three adsorbates.

Figs. 6 and 7 show the number density of molecules in MCM-41 with pore diameter of 2.2 and 3.2 nm as a function of distance from the pore axis, respectively. The dotted line corresponds to the number density of molecules just below the capillary-condensation pressure. The figures clearly show that at high P/P_{sat} 2 and 3 layers of the molecules are formed in MCM-41 with pore diameter of 2.2 and 3.2 nm, respectively. It is notable that the number of peaks at high P/P_{sat} is constant in a given pore for the three adsorbates, and that the positions of peak are almost constant for the three adsorbates regardless of the pore diameter. The peaks of carbon tetrachloride are less smooth compared to those of neopentane and cyclohexane, suggesting that the adsorptive sites of MCM-41 interacting with carbon tetrachloride are more than those interacting with neopentane or cyclohexane. In general, a multilayer of molecules appears after the molecules form monolayer at very low P/P_{sat} in nanopore, and then the molecules fill rapidly at the capillary-condensation pressure. The isotherms are nearly flat above the capillary-condensation pressure. As shown in Figs. 6 and 7, at low P/P_{sat} the adsorption behavior of the molecules differs from the typical behavior of adsorption mentioned above. The carbon tetrachloride and neopentane molecules form weak monolayers in MCM-41 with pore diameter of 3.2 nm just below the capillary-condensation pressure, and the cyclohexane molecules do not form even the monolayer below the capillary-condensation pressure, which is probably because the pore is not large enough to form layers for the three adsorbates below the capillary-condensation pressure. For instance, Ravikovitch et al. reported that toluene formed a disordered multilayer in MCM-41 with pore diameter of 4.5 nm below the capillary-condensation pressure [32].

The views of snapshots for the center-of-points of molecules in MCM-41 with pore diameter of 3.2 and 2.2 nm at about saturated vapor pressure are shown in Figs. 8 and 9. Fig. 8 shows that the carbon tetrachloride molecules confined in pores are ordered along the pore axis. However, neopentane and cyclohexane molecules do

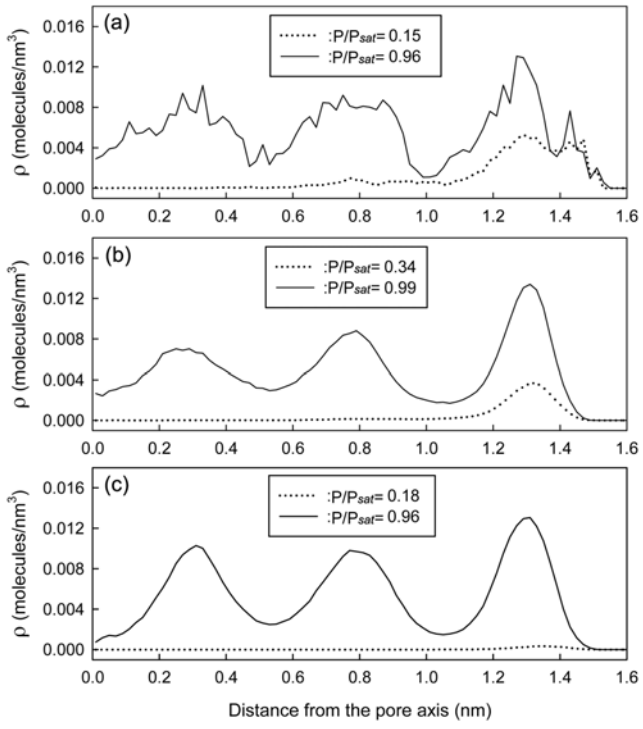

Fig. 7. As in Fig. 6 but for MCM-41 with pore diameter of 3.2 nm.

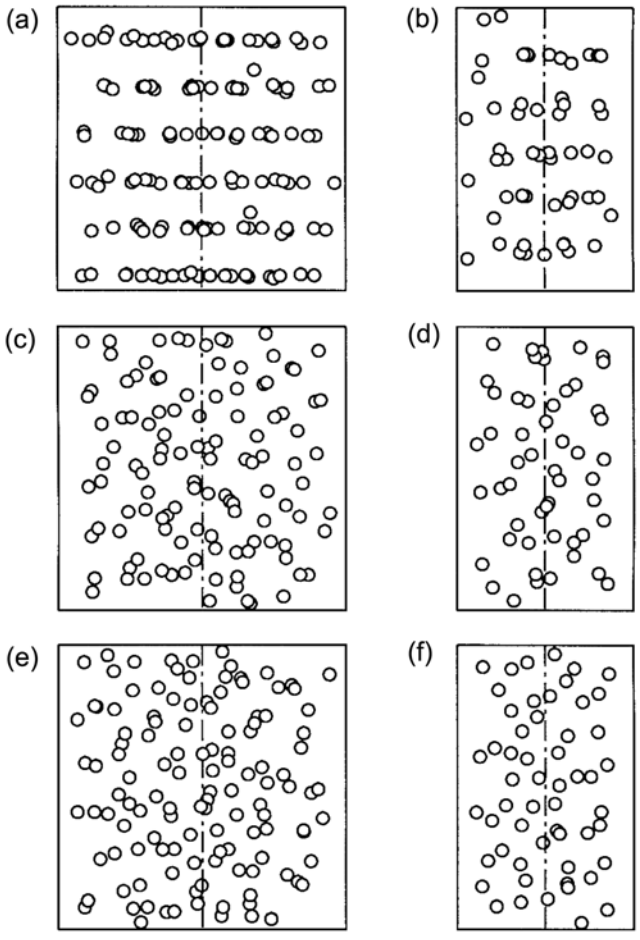

Fig. 8. Lateral views of snapshots for the center-of-mass points of molecules in MCM-41 with pore diameter of 3.2 (left) and 2.2 nm (right): (a) carbon tetrachloride at 298 K and P/P_{sat}= 0.96, (b) carbon tetrachloride at 298 K and P/P_{sat}=0.97, (c) neopentane at 273 K and P/P_{sat}=0.99, (d) neopentane at 273 K and P/P_{sat}=0.99, (e) cyclohexane at 298 K and P/P_{sat}=0.96, (f) cyclohexane at 298 K and P/P_{sat}=1.00. Dash-dot line denotes the pore axis.

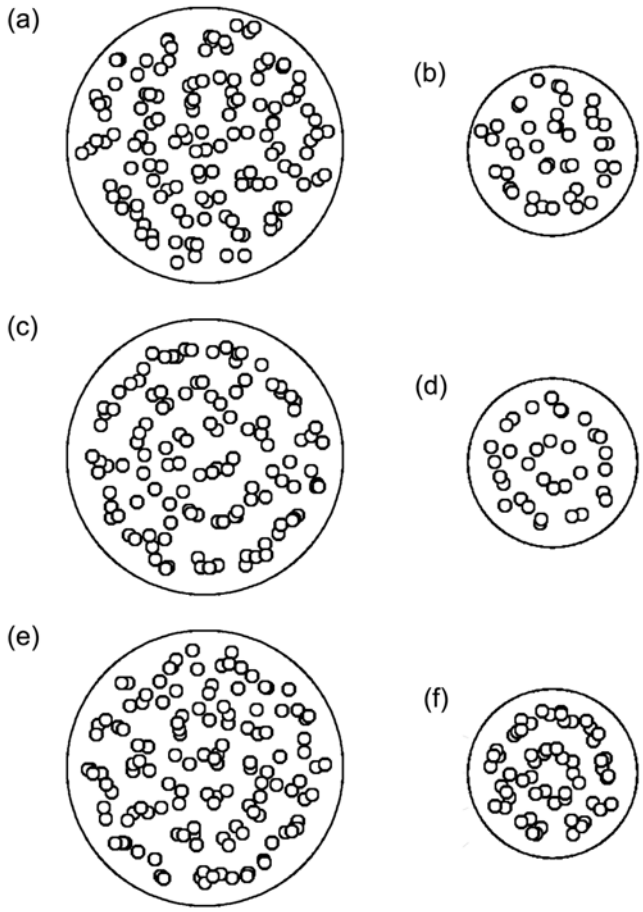

Fig. 9. Top views of snapshots for the center-of-mass points of molecules in MCM-41 with pore diameter of 3.2 (left) and 2.2 nm (right): (a) carbon tetrachloride at 298 K and P/P_{sat}= 0.96, (b) carbon tetrachloride at 298 K and P/P_{sat}=0.97, (c) neopentane at 273 K and P/P_{sat}=0.99, (d) neopentane at 273 K and P/P_{sat}=0.99, (e) cyclohexane at 298 K and P/P_{sat}=0.96, (f) cyclohexane at 298 K and P/P_{sat}=1.00.

not form this arranged structure. The carbon tetrachloride molecules in MCM-41 with pore diameter of 3.2 nm are more ordered than those with pore diameter of 2.2 nm. Similarly, ordering of water molecules in single-walled carbon nanotubes was reported [33]. We plotted the number density of carbon tetrachloride molecules in MCM-41 as a function of distance along the pore axis in Fig. 10, which clearly shows ordering phenomenon of carbon tetrachloride molecules. The distances between layers are about 0.5 nm regardless of pore diameter.

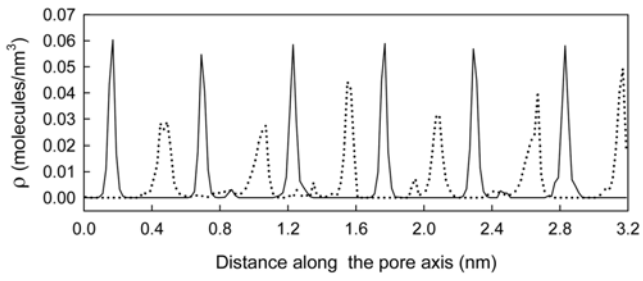

Fig. 10. Number density of carbon tetrachloride molecules at 298 K, ρ, in MCM-41 as a function of distance along the pore axis: solid line, at P/P_{sat}=0.96 for pore diameter of 3.2 nm; dot line, at P/P_{sat}=0.97 for pore diameter of 2.2 nm.

CONCLUSIONS

GCMC simulations were performed to study the adsorption properties of carbon tetrachloride, neopentane, and cyclohexane in MCM-41 with pore diameter of 2.2 and 3.2 nm. The pore model with amorphous silica surface was used in simulation. The capillary-condensation pressures increased as the pore diameters increased. The simulated adsorption amounts of neopentane above the capillary-condensation pressure agreed with the experimental ones. However, those of carbon tetrachloride above the capillary-condensation pressure were less than the experimental ones. The average densities of carbon tetrachloride, neopentane, and cyclohexane in the two different pores above the capillary-condensation pressure were smaller than the corresponding liquid densities by about 12%.

The microstructures of adsorbate molecules in the pore of MCM-41 were investigated. The carbon tetrachloride and neopentane molecules formed weak monolayers, and the cyclohexane molecules did not form monolayer below the capillary-condensation pressure. Above the capillary-condensation pressure, 2 and 3 layers of the adsorbate molecules were formed in MCM-41 with pore diameter of 2.2 and 3.2 nm, respectively. In addition, the carbon tetrachloride molecules confined in pore were also ordered along the pore axis.

ACKNOWLEDGMENT

This work was financially supported by Dongeui University.

NOMENCLATURE

b : trial position
B : virial coefficient
e : electronic charge
f : fugacity of the vapor phase
d_{pe} : pore diameter in experiment
d_{ps} : pore diameter in simulation
k : Boltzmann constant
m : total number of trials
N : number of molecules in simulation box
N_{ox} : number of oxygen atoms
N_{si} : number of silicon atoms
P : pressure
P_{sat} : saturated vapor pressure
P_{acc} : acceptance probability
q : partial charge
q_{st} : isosteric heat
R : gas constant
r : distance
T : temperature
u : energy
U : potential of adsorbate
V : volume of simulation box

$W^{(n)}$: new Rosenbluth factor
$W^{(o)}$: old Rosenbluth factor
x, y, z : coordinate axis

Greek Letters

β : 1/kT
ε : potential parameter
ρ : number density of molecules
σ : potential parameter
ϕ_{sm} : potential between a site of adsorbate molecules and MCM-41

Subscripts

a, *b* : site
i : growth step
j : particular trial

REFERENCES

1. X. S. Zhao, G. Q. Lu and G. J. Millar, *Ind. Eng. Chem. Res.*, **35**, 2075 (1996).
2. P. Selvam, S. K. Bhatia and C. G. Sonwane, *Ind. Eng. Chem. Res.*, **40**, 3237 (2001).
3. A. Z. Panagiotopoulos, *Mol. Simulation*, **9**, 1 (1992).
4. B. Smit and J. I. Siepmann, *J. Phys. Chem.*, **98**, 8442 (1994).
5. K. Chihara, C. F. Mellot, A. K. Cheetham, S. Harms, H. Mangyo, M. Omote and R. Kamiyama, *Korean J. Chem. Eng.*, **17**, 649 (2000).
6. B.-H. Kim, G-H. Kum and Y.-G. Seo, *Korean J. Chem. Eng.*, **20**, 104 (2003).
7. A. J. P. Carvalho, T. Ferreira, A. J. E. Candeias and J. P. P. Ramalho, *J. Mol. Struct. (Theochem)*, **729**, 65 (2005).
8. J. P. Fox and S. P. Bates, *Langmuir*, **21**, 4746 (2005).
9. M. W. Maddox, J. P. Olivier and K. E. Gubbins, *Langmuir*, **13**, 1737 (1997).
10. C. A. Koh, T. Montanari, R. I. Nooney, S. F. Tahir and R. E. Westacott, *Langmuir*, **15**, 6043 (1999).
11. J.-H. Yun, T. Duren, F. J. Keil and N. A. Seaton, *Langmuir*, **18**, 2693 (2002).
12. Y. He and N. A. Seaton, *Langmuir*, **19**, 10132 (2003).
13. D. Cao, Z. Shen, J. Chen and X. Zhang, *Microporous and Mesoporous Mater.*, **67**, 159 (2004).
14. B. Kuchta, P. Llewellyn, R. Denoyel and L. Firlej, *Colloids Surf. A*, **241**, 137 (2004).
15. B. Kuchta, R. Denoyel and L. Firlej, *Colloids Surf. A*, **241**, 143 (2004).
16. X. Yang and X. Yue, *Colloids Surf. A*, **301**, 166 (2007).
17. B. Coasne and R. J.-M. Pellenq, *J. Chem. Phys*., **120**, 2913 (2004).
18. B. Coasne, F. R. Hung, R. J.-M. Pellenq, F. R. Siperstein and K. E. Gubbins, *Langmuir,* **22**, 194 (2006).
19. B. W. H. van Beest, G. J. Kramer and R. A. van Santen, *Phy. Rev. Lett.*, **64**, 1955 (1990).
20. J. J. de Pablo, M. Bonnin and J. M. Prausnitz, *Fluid Phase Equilibria*, **73**, 187 (1992).
21. R. Rey, L. C. Pardo, E. Llanta, K. Ando, D. O. Lopez, J. L. Tamarit and M. Barrio, *J. Chem. Phys*., **112**, 7505 (2000).
22. A. Gupta, L. A. Clark and R. Q. Snurr, *Langmuir*, **16**, 3910 (2000).
23. B. Smit, *Mol. Phys.*, **85**, 153 (1995).
24. J. R. Errington and A. Z. Panagiotopoulos, *J. Chem. Phys*., **111**, 9731 (1999).
25. M. G. Martin and J. I. Siepmann, *J. Phys. Chem. B*, **103**, 4508 (1999).
26. M. D. Macedonia and E. J. Maginn, *Mol. Phys*., **96**, 1375 (1999).
27. D. R. Lide and H. V. Kehiaian, *CRC handbook of thermophysical and thermochemical data*, CRC Press, Boca Raton (1994).
28. M. Hakuman and H. Naono, *J. Colloid Interface Sci.*, **241**, 127 (2001).
29. M. M. L. R. Carrott, A. J. E. Candeias, P. J. M. Carrott, P. I. Ravikovitch, A. V. Neimark and A. D. Sequeira, *Microporous and Mesoporous Mater*., **47**, 323 (2001).
30. E. A. Muller, F. R. Hung and K. E. Gubbins, *Langmuir*, **16**, 5418 (2000).
31. D. R. Lide, *CRC handbook of chemistry and physics*, CRC Press, Boca Raton (1999).
32. P. I. Ravikovitch, A. Vishnyakov, A. V. Neimark, M. M. L. R. Carrott, P. A. Russo and P. J. Carrott, *Langmuir*, **22**, 513 (2006).
33. A. Striolo, A. A. Chialvo, K. E. Gubbins and P. T. Cummings, *J. Chem. Phys.*, **122**, 234712 (2005).